Journal of Energy Storage 23 (2019) 19–28

Contents lists available at ScienceDirect

Journal of Energy Storage

journal homepage: www.elsevier.com/locate/est

Battery energy storage system modeling: Investigation of intrinsic cell-to-cell variations

Matthieu Dubarry[a,*], Carlos Pastor-Fernández[b], George Baure[a], Tung Fai Yu[c], W. Dhammika Widanage[b], James Marco[b]

[a] Hawai'i Natural Energy Institute, SOEST, University of Hawai'i at Mānoa, 1680 East-West Road, POST 109, Honolulu, HI 96822, USA
[b] WMG, University of Warwick, Coventry, CV4 7AL, UK
[c] Jaguar Land Rover, Banbury Road, Warwick, CV35 0XJ, UK

ARTICLE INFO

Keywords:
Li-ion batteries
Cell-to-cell variations
Inhomogeneities
Pack modeling
Series
Parallel
Battery energy storage system

ABSTRACT

Cell-to-cell variations can drastically affect the performance and the reliability of battery packs. This study provides a model-based systematic analysis of the impact of intrinsic cell-to-cell variations induced by differences in initial state of charge, state of health, capacity ration, resistance and rate capability. The impact of these cell-to-cell variations was evaluated on the performance of battery packs of different topologies, from series to parallel, and chemistries. For each chemistry and topology, simulations were performed with different levels for each type of intrinsic variation as well as all variations together in order to investigate the combined effects. The most salient changes were observed for cells connected in series. The calculated incremental capacity response for the pack and the single cells was used to select different features of interest that changed depending on the type of variation. From this methodology, the automatic quantification of the variations was attempted at the pack and single cell level. Cell-to-cell variations make each battery pack unique; their quantitation is essential for accurate monitoring.

1. Introduction

In order to meet energy and power requirements, vehicle battery packs typically comprise a high number of cells connected in series and parallel. Battery pack performance can be altered by several factors, both intrinsic and extrinsic. Intrinsic factors are defined as inconsistencies in materials and in manufacturing processes [1,2]. Extrinsic factors include those caused by the environment, e.g., different calendar age for single cells, and non-uniform current or temperature distributions [1,3]. Altogether, these inconsistencies could be referred as cell-to-cell variations (CtCV) [4,5]. CtCV are quite common despite efforts to mitigate them by improving battery designs, manufacturing, and quality control processes as well as by battery management system regulations. To optimize battery pack performance, and ensure proper control, it is desirable to understand and quantify these variations. Several methodologies have been proposed before assembly [1,6] but limited work has been done on a practical method to quantify CtCV after assembly. Since CtCV makes each battery pack unique, quantifying their extent and determining their origins within the battery management system (BMS) would increase the overall accuracy of the battery pack balancing [7], state of charge (SOC), and state of health (SOH) tracking algorithms [8–11].

A discussion on the origins of the CtCV is out of the scope of this paper. For such a discussion, the reader is referred to an article by Rumpf et al. [1]. The extent of initial CtCV within a batch of cells, although not reported often enough, has been the topic of multiple studies in the literature [1,4–6,12–30]. For the nominal capacity, most reported variations were below ± 5% although some higher variations were reported [29]. Looking at the initial SOC, some studies reported variations below ± 5% [6,20,26], while others reported higher variations of ± 8.5% [27] or above [29,30]. However, in the latter case, the cells were over 7 years old [30] and thus suffered significant self-discharge. For the ohmic resistance, variations were found to range between ± 3% [30] and ± 30% [19]. Rate capability variations, the ratio of the nominal capacity to the maximum capacity, were reported to be ± 0.1 [20] and ± 3% [6]. Maximum capacity variations were between ± 0.2% [20] and ± 1.5% [6] and SOH variations around ± 0.5% [26,27].

CtCV could drastically influence the assembly performance and durability [29,31–33]. Most studies on pack modeling noted the effect of CtCV on the battery performance [28,34–37], but few proposed methods to foresee their impact. Using a modified multi-Equivalent

* Corresponding author.
E-mail addresses: matthieu.dubarry@gmail.com (M. Dubarry), carlos.pastor@warwick.ac.uk (C. Pastor-Fernández), tyu5@jaguarlandrover.com (T.F. Yu).

https://doi.org/10.1016/j.est.2019.02.016
Received 9 December 2018; Received in revised form 23 January 2019; Accepted 13 February 2019
Available online 08 March 2019

Circuit Model (ECM) approach, we previously investigated the impact of CtCV for single cells (SC) in series [38] and parallel [39]. Zhou et al. [40,41] and Zhang et al. [29] studied the impact of different parameters, such as manufacturing variations and self-discharge rates, using a set of standard ECMs in series. Miyatake et al. [18] have experimentally evaluated the influence of capacity CtCV on the discharge capacity for different module topologies, both series and parallel, but did not investigate any other parameters. Jiang et al. [33] measured cell variations of a 95S5P 18.5 kWh LFP battery pack after aging and showed a maximum of 7% SOC variation reduced the maximum available capacity of the pack by 25%. Paul et al. [24] studied initial nominal capacity and resistance variations. Quantifying the mean and the standard deviation, Zhang et al. [29] analyzed the effect of capacity and SOC CtCV in a 104S3P battery pack and found that SOC variations had a significant impact on pack capacity. Zhou et al. [41] developed a 96S1P LFP battery pack model to evaluate the impact of CtCV. The results revealed that performance was mainly affected by the coulombic efficiency (loss of lithium inventory), self-discharge rate, and temperature. They claimed that the initial parameters (capacity, SOC and resistance) as well as the resistance growth with aging have little effect on capacity fade. This finding opposed other studies [24,33]. More recently, Rumpf et al. [37], used multiphysics multidimentional modeling to look for the impact of capacity, resistance, and temperature on the performance of battery packs of different topologies.

Through statistical analysis or simulations, previous literature investigated the effect of CtCV induced by temperature, SOC, resistance, capacity and coulombic efficiency. However, none of these studies proposed a systematic study of the different sources of CtCV and their combined impact on the cell voltage response and capacity, independently of the cell chemistry and the topology. This work is aimed at characterizing the impact of different types and levels of CtCV occurring at the same time on battery packs of different topologies and chemistries and at providing a framework to investigate the relationship between cell quality and performance without requiring extensive testing. Initial variations of maximum capacity, SOC, SOH, resistance and rate capability were considered. This methodology was repeated on three of the most common Li-ion cell chemistries and on the three main battery pack topologies comprising cells in series and/or parallel. This study focused on CtCV that were pertinent to new battery packs and used the battery pack model presented in a previous publication [42]. The changes in voltage response were discussed from an incremental capacity (IC) point of view [43] using the feature of interest approach [8].

2. Experimental

All simulations performed in this work were undertaken using the *Hanalike* model described in detail within our previous work [42] and summarized in Fig. 1. The model combines several previously published and validated models. The use of the *alawa* toolbox [44,45] allows simulating cells with different chemistries and age based on half-cell data. The *apo* and *ili* ECM models allows simulating cells with different amounts of active material, morphologies, and resistance [46]. Based on the topology, the data is then handled by *kaulike* [39] for paralleling and by *anakonu* [3] for cells or modules connection in series.

In this investigation, battery packs consisting of 49 single cells were simulated for three chemistries and three topologies. The number of single cells was chosen to be large enough to be representative of large battery packs, while small enough to limit calculation time. For each chemistry and topology, the five most common types of CtCV based on our literature survey were simulated, each at five levels of intensity. The total number of unique simulations considered in this work was 450 (225 packs for 2 different rates).

The three chosen chemistries consisted of graphite intercalation compound (GIC) as the negative electrode with $LiMn_2O_4$ (LMO), $LiAl_xNi_yCo_{1-x-y}O_2$ (NCA) and $LiFePO_4$ (LFP) as positive electrodes. All these chemistries are commercially available and considered for either transportation or storage applications. For convenience, since the negative electrodes are the same in all three cases, the cells were referred to by their positive electrodes. The data was obtained from electrodes harvested from commercial cells. The electrodes were tested in half-cell configurations versus metallic lithium. Additional details on the cells as well as the disassembly and testing procedures are out of the scope of this paper and can be found in [3] for LMO, [26,47] for NCA, and [48,49] for LFP. The cells specifications, including nominal voltages and cutoffs, are summarized in Table 1.

The three investigated topologies were nS1P, 1SmP and mPnS. In the nS1P configuration, the 49 cells are connected in series. In the 1SmP configuration, the 49 cells were connected in parallel. This configuration is usually used in laptops or notebooks [50,51]. In the mPnS configuration, the 49 cells were organized as 7 cells in parallel forming one of the 7 modules connected in series. Similar to the nSmP configuration, this topology optimizes output energy and power but, as cells are not connected in series then paralleled, the mPnS topology can be used even if one cell failed. Hence, the mPnS configuration is the preferred topology for automotive applications, e.g. in the Tesla Model S [52], and it was thus chosen over the nSmP topology for this study.

For each battery pack, five types of intrinsic CtCV were considered, Table 2. First, the initial SOC variation (SOCi) which can occur when cells were not charged to the same open circuit voltage at the end of the formation step. In this paper, SOC was defined as the ratio between the available and the maximum capacity. The second CtCV considered was the single-cell state of health (SOH). These inhomogeneities can be introduced by using cells with different calendar ages (stored for different amounts of time or in different conditions). In this work, it was assumed that calendar aging was driven solely by loss of lithium inventory whose impact was emulated using the 'alawa toolbox [44,45]. SOH was defined as the ratio between the capacity at a given SOH and

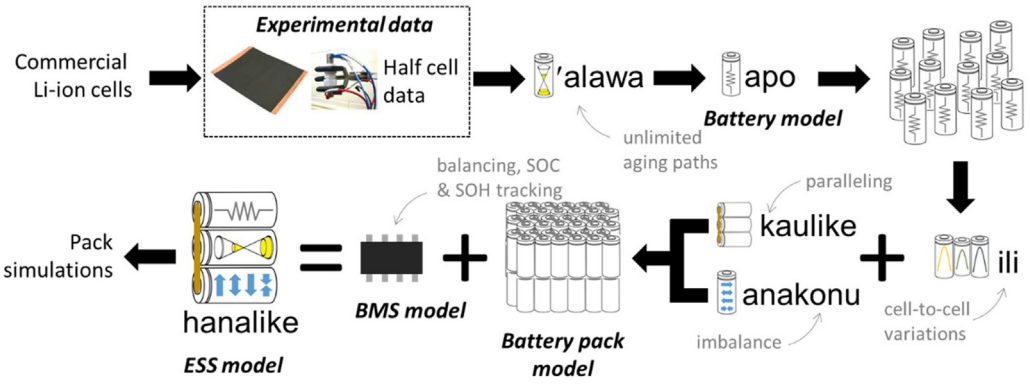

Fig. 1. Schematic representation of the Hanalike model.

Table 1
Specifications of cell chemistries.

Cathode material	LMO	NCA	LFP
Anode material	GIC	GIC	GIC
Nominal voltage	3.5 V	3.35 V	3.075 V
Charge cut-off voltage	4.2 V	4.2 V	3.65 V
Discharge cut-off voltage	2.8 V	2.9 V	2.5 V
Original publication	[3]	[26,47]	[48,49]

Table 2
Cell-to-cell variations summary.

	Abbr.	Definition	Range
Initial SOC	SOCi	From initial open circuit voltage	± 5%
SOH	SOH	Maximum capacity/maximum capacity fresh cell	± 5%
Capacity ration	Qr	Maximum capacity/100	± 5%
Ohmic resistance	R	From ohmic drop when current is applied	± 15%
Rate capability	RC	Nominal capacity/maximum capacity	± 5%

the capacity at 100% SOH. The third CtCV studied was the capacity ration (Qr) in mAh/%SOC, a proxy to the cell maximum capacity (i.e. the capacity for 100% SOC). Variations in Qr can occur when batteries have differences in electrode size or loading [6]. Variations in ohmic resistance (R) were also considered. They can arise from battery intrinsic parameters such as separator thickness or extrinsic ones such as connections with terminals. Finally, variations in rate capability (RC) were investigated. They can originate from variations of the electrode architecture [2] affecting the power ability. RC was defined as the ratio between the C/2 nominal capacity and the maximum capacity. In addition, simulations were undertaken with all CtCV (All) occurring at the same time to investigate combined effects.

Simulations were all started with a small rest from a fully charged state and were stopped when the discharge cutoff voltage was reached at the single cell or pack level. C/25 discharges were used to evaluate the impact of SOCi, SOH and Qr with five levels of variations, 0%, ± 1.25%, ± 2.50%, ± 3.75%, ± 5.00%. C/2 simulations were used to study of the effect of R and RC variations to magnify their influence. For R, the extent of the CtCV was increased to 0%, ± 3.75%, ± 7.50%, ± 12.50%, ± 15.00% to better match the literature. Values for the CtCV parameters (SOCi, SOH, Qr, R, RC, or all) were chosen randomly within a normal distribution. The normal distribution ensured that the average values were the same for all battery packs independently of the amplitude and the nature of the cell-to-cell variations. Additionally, it more closely represented reality [13,24,28,29,33] than a full random selection. The different CtCVs were considered independent of each other to the exception of SOH variations that induces Qr variations as capacity is lost. Since SOCi, SOH and RC values above 1 were not physically possible, the average value for these parameters was chosen to be 95% instead of 100% so that ± 5% simulations were achievable. To mitigate the possible impact of the random values, all simulations were repeated up to 30 times. There was little difference in the results from 30- and 10-repetition experimental designs. Consequently, a 10-repetition experiment was chosen to limit simulation times. The iteration times for the model [42] were set at 1/300th the selected rate for simulations in parallel, 1/1500th the simulated rate for simulations in series and 1/20th of the relaxation time. This varying iteration time is used to perform simulations based on the number of points per charge or discharge and not time.

3. Results

The slight variation of voltage induced by the CtCV is difficult to describe on a voltage vs. capacity curve because of the large voltage window. To circumvent this issue, a derivative of the curve, IC ($dQ/dV = f(V)$, [43]) is used in the rest of this work to enhance the visibility of the voltage variations. Fig. 2 presents the C/25 battery packs IC curves (IC_P) associated with the variations of SOCi, SOH, Qr, and all (rows) as function of the pack topology (columns) for the LMO battery. The curves are the average of the 10 repetitions for each set of conditions. Standard deviations were on average below 0.5%. Similar figures for the NCA and LFP batteries are provided in supplementary Fig. S1. Overall, the CtCV had little impact on the voltage response of the cell with only some slight variations at high voltage, feature of interest

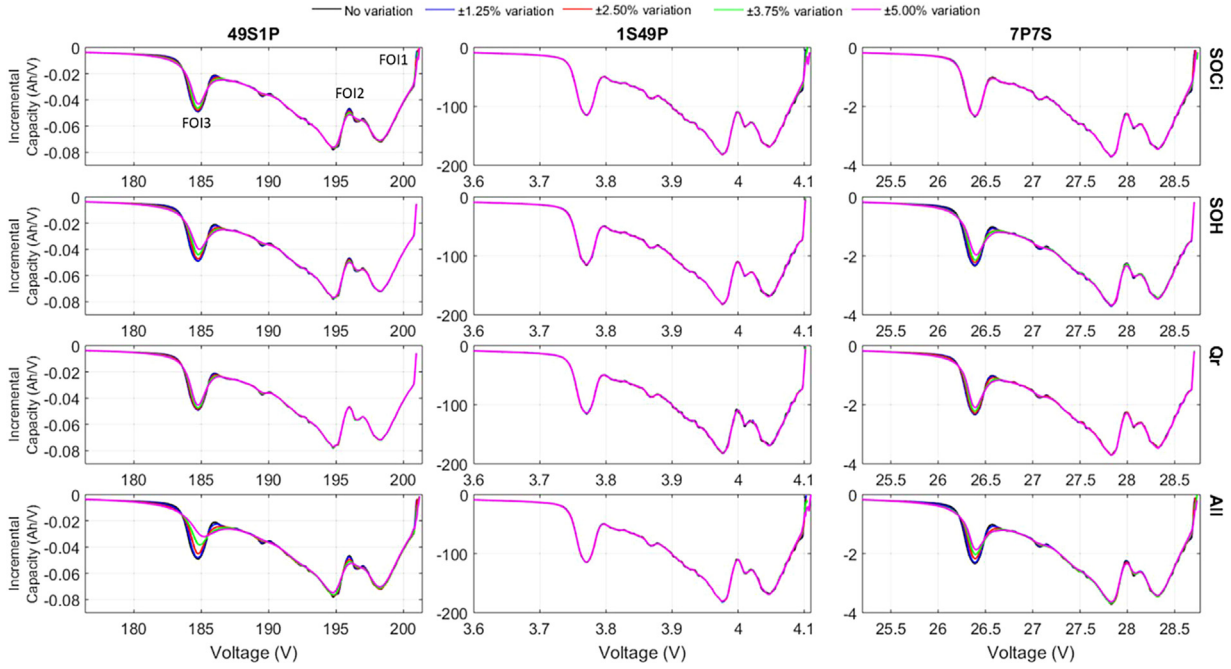

Fig. 2. LMO C/25 average voltage variations (10 repetitions) induced by SOCi, SOH, Qr, and All CtCV for the three simulated topologies. Areas with the most variations were deemed to be a feature of interest (FOI) and labeled as FOI1, FOI2 and FOI3.

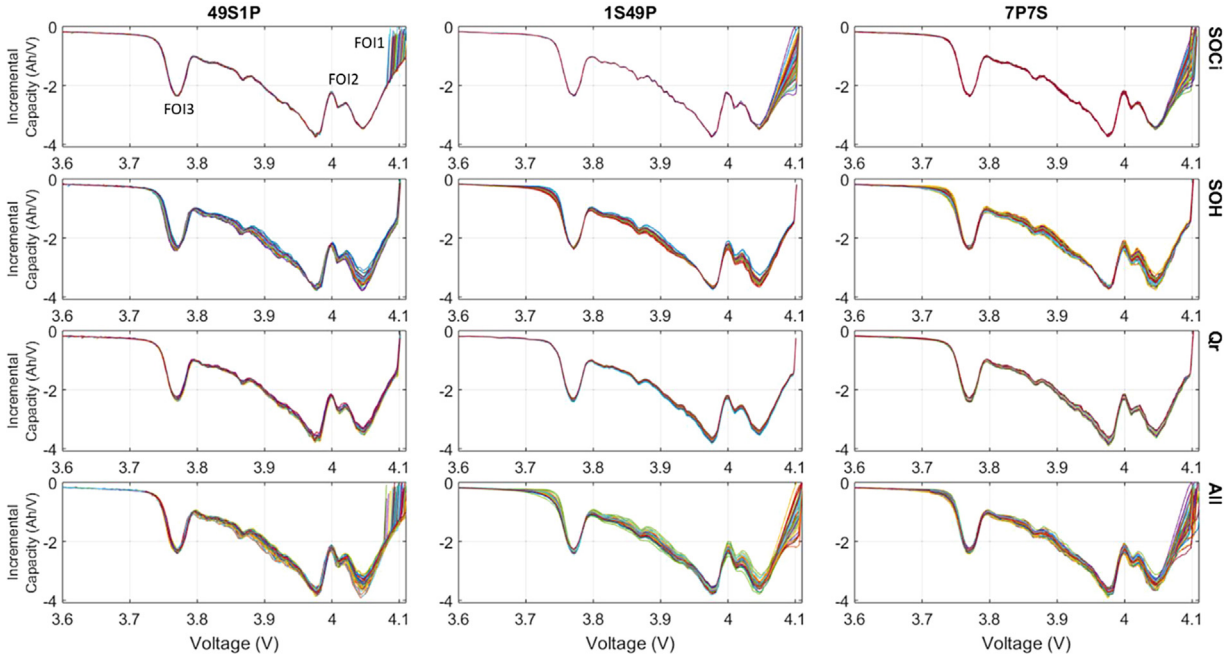

Fig. 3. ± 5% LMO C/25 variations induced by SOCi, SOH, Qr, and All CtCV for the three simulated topologies and the 49 single cells. Different colors correspond to different single cells. Areas with the most variations were deemed to be a FOI and labeled as FOI1, FOI2 and FOI3.

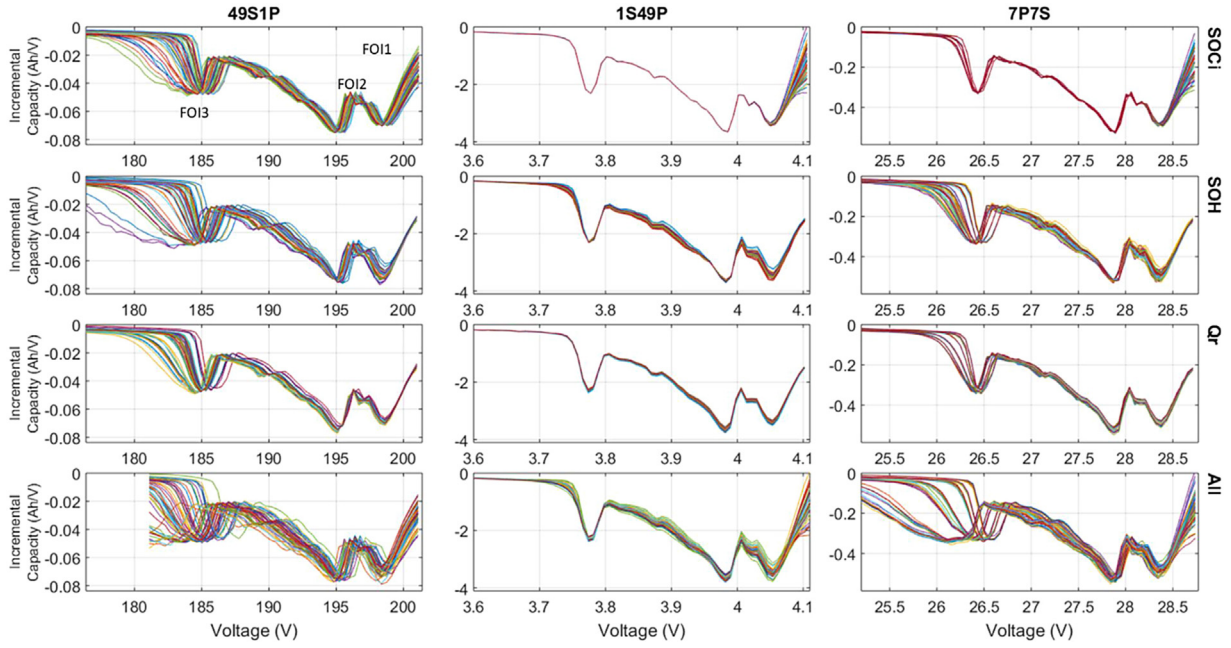

Fig. 4. ± 5% LMO C/25 variations induced by SOCi, SOH, Qr, and All CtCV for the three simulated topologies and the 49 single cells plotted as a function of pack voltage instead of single cell voltages. Different colors correspond to different single cells. Areas with the most variations were deemed to be a FOI and labeled as FOI1, FOI2 and FOI3.

(FOI) 1, an intensity decrease in-between the two high voltage peaks (FOI2) and, most significantly, a broadening of the low voltage peak (FOI3).

For SOCi variations (first row of graphs in Fig. 2), only the 49S1P configuration exhibited a substantial change to the IC curves. The changes to FOI2 and FOI3 were particularly noticeable. For all the other variations, similar changes can be observed for 49S1P and 7P7S (first and third columns of graphs in Fig. 2). The only difference was the intensity of the changes. The SOH CtCV had a larger impact on the 49S1P topology than the 7P7S topology; while, for the Qr variation, the inverse was true. In contrast, the voltage response from the 1S49P simulation showed no observable change attributable to the CtCV. Similar observations were made for the NCA and LFP batteries at C/25 (Fig. S1).

Fig. 3 presents the C/25 single cells IC signatures (IC_{SC}) for the ± 5% LMO simulations as a function of the topologies (columns) and the CtCV (rows). Similar data for the NCA and LFP batteries are presented in Fig. S2. Looking at SOCi variations, the impact at the SC level depended on the topology. For the series configuration, discharges started at different voltages based in the initial SOC. For configurations with paralleling, all SC started at the same voltage but the usage was different until the balancing between the cells was completed in the

middle of the high voltage peak. IC curves were overlapping at lower voltages because, besides the initial SOC, the cells were identical. In contrast, the SOH variations modified the entire voltage response of the cell. The impact of SOH variations without balancing can be seen in the voltage response of the 49S1P configuration. The intensity of first high voltage peak was most affected by the SOH CtCV. The position of the low-voltage peak shifted toward higher voltages. Putting cells with different SOH in parallel broadened all the peaks. In comparison to the change induced by variations in the SOH of the cells, the changes on the SC level induced by Qr were slight. This relatively small effect was expected because the variations affected all peaks uniformly and thus, the changes were less visible. It should be noted that the values were centered around the average with a normal distribution; therefore, a few cells did have large deviations from the average. For the variations of all parameters at the same time, the sum of all the previous observations were seen. Similar observations were made for the NCA and LFP batteries (Fig. S2).

Fig. 4 displays the IC signatures of the SC at the pack level for the LMO simulations as a function of the topologies (columns) and CtCV (rows) where the x-axis is the pack voltage instead of the single cell voltage ($IC_{SC/P}$) as in Fig. 3. As explained in our previous work where the model was introduced [42], this $IC_{SC/P}$ representation highlighted the usage of the different SCs and differentiated the variations observed in the IC curves for the battery packs. Similar data for the NCA and LFP batteries are presented in Fig. S3. The high voltage changes resembled the ones in Fig. 3 but, in this representation, the origin of the broadening of FOI3 was clearly visible. For some of the single cells, FOI3 was significantly affected. This observation could not be made from Fig. 3 because some cells finished their discharge before others. Toward the end of discharge, the voltages of the cells that were already fully discharged decreased rapidly compared to the others in the pack. As a result, the pack voltage decreased rapidly and FOI3 broadened for the cells that were yet to complete this electrochemical process. The discrete grouping for the 7P7S simulations was induced by the fact that there are 7 strings and thus only 7 different currents for the 49 cells.

For interested readers, the differential voltage curves (dV/dQ) associated with this study are included in Fig. S4 for the LMO cell, in Fig. 5 for the NCA cell, and in Fig. S6 for the LFP cell. The variations shared similitudes with the IC analysis and did not provide any additional information.

Fig. 5 shows the voltage response of an NCA battery pack discharged at C/2 with up to ± 15% R variations and ± 5% RC variations. Fig. S7 presents the voltage response of LMO and LFP cell with up ± 15% R variations. The influence of the other CtCVs was similar at C/25 (not shown). RC changes of ± 5% could not be properly taken into account by the model for LMO and LFP. As explained in a previous publication [42], RC changes were determined by scaling the rate vs. normalized capacity curve so that the nominal capacity corresponded to the RC. However, this scaling could not be performed for the LMO and LFP cells in this study because these high-power electrodes exhibited too small a capacity difference between the rates tested in this experiment.

Both R and RC variations did not influence the voltage signature of the battery pack except for LMO where FOI3 was slightly affected, Fig. S7. Looking at the 49S1P IC_{SC} curves for all chemistries, changes of resistances shifted the IC curves along the voltage axis but their usage was the same as proven by the overlapping $IC_{SC/P}$ curves. However, for the 1S49P, the resistance variations had a different impact with different intensity for the IC peaks. The 7P7S battery pack exhibited a combination of both behaviors. Changes in rate capability did not noticeably affect the shape of the voltage response of the SC and, by extension, of the battery pack except when the cells were connected in series where some slight differences were visible.

4. Discussion

The model was successful in simulating all the different conditions. Fig. 6 presents the capacity retention differences associated with all simulations for the LMO, NCA and LFP cells arranged in all topologies at C/25. It must to be noted again that the average values for all parameters were the same despite any variation. At first glance, it appeared that the 49S1P configuration was more prone to capacity retention differences induced by CtCV (8% at most) than the 7P7S (5%), and the 1S49P (< 1%) configurations. However, looking into more detail at the individual CtCV data, the impact of SOCi in the 49S1P configuration was similar for all three chemistries and accounted for a 3% difference on average in capacity retention for the ± 5% variations. For the 7P7S topology, the loss was the same for LFP and below 1% for LMO and NCA. The SOH CtCV induced up to 8% deviation in the capacity retention for the 49S1P configuration regardless of the cell chemistry. For the 7P7S configuration, the deviations were of 5% for LFP, 3% for LMO and 1% for NCA. The effect of SOH was also the most substantial for each case (Fig. 6). For the capacity ration, the deviation was around 3% in series for all three chemistries; while, it was 2.5% in the 7P7S configuration for the LMO and LFP chemistries and close to 0 for NCA. In all cases, the retention was worst when all CtCV varied at the same time (All), which indicated there were combined effects. Overall, the impact of CtCV was similar for all chemistries with NCA being the least susceptible of the three. The maximum difference in capacity retention was recorded for the serial configuration at around 15% for one of repetition when all CtCVs varied at the same time. This finding highlighted how combined variations in the ± 5% range could drastically affect the performance of a battery pack. At ± 3.75% and ± 2.5% variations, the maximum deviations were 11% and 6%, respectively, in the serial configuration. For the 7P7S configuration, the maximum deviation was around 8%. The ± 15% R variations did not result in any change on the capacity retention irrespective of the chemistry and the topology. The ± 5% RC variations induced between 2 and 4% capacity loss for NCA-based battery pack with the cells in series (not shown).

The model also provided the variation of rate at the single-cell level. This capability may be particularly useful for the battery packs with cells connected in parallel because it will provide information on the internal balancing. The rate variations for the C/25 LMO simulations are shown in Fig. 7. The variations for the C/25 NCA and LFP simulations are provided in supplementary Fig. S8. The visualization of the rate enabled the analysis of the internal balancing within the battery packs and complemented the observations from Figs. 3 and 4. For packs with SOC_i CtCV, most of the variations were within the first five hours during which balancing brought each of the cells to the same SOC. Some changes were also visible toward end of discharge for the 7S7P simulations. These changes were likely induced by disparities between properties of the cells in the string. For instance, some cells might be closer to end of discharge than others and hence, would exhibit greater voltage variations. The impact of variations of Qr were also easily explained. Since variations in Qr only modified the amount of active material, the rate was mostly stable but slightly different for each SC. Variations of SOH produced more complex current balancing because SOH CtCV induced changes in the voltage response of the cell. Since voltage must be constant across the parallel configuration, balancing was necessary at all SOCs depending on the SOH-induced voltage changes. The All rate variations corresponded to a mix of the effects of the three CtCV types which held true for all chemistries including NCA and LFP (Fig. S8). In the mid SOC range, once balancing is complete, the rate of discharge differences between cells are oscillating along the phase transformations in the electrodes, i.e. following the IC peaks. This is especially visible for SOH variations in LFP (Fig. S8) because of the well-defined voltage plateaus requiring more accommodation (steep voltage changes). These rate differences could induce some temperature gradients in the pack and thus lead to inhomogeneous aging. This will be investigated once a thermal component is added to the model.

Looking at the R and RC CtCVs, Fig. 8, the rate variations occurred at different SOCs. For R, there was more discrepancy at the beginning

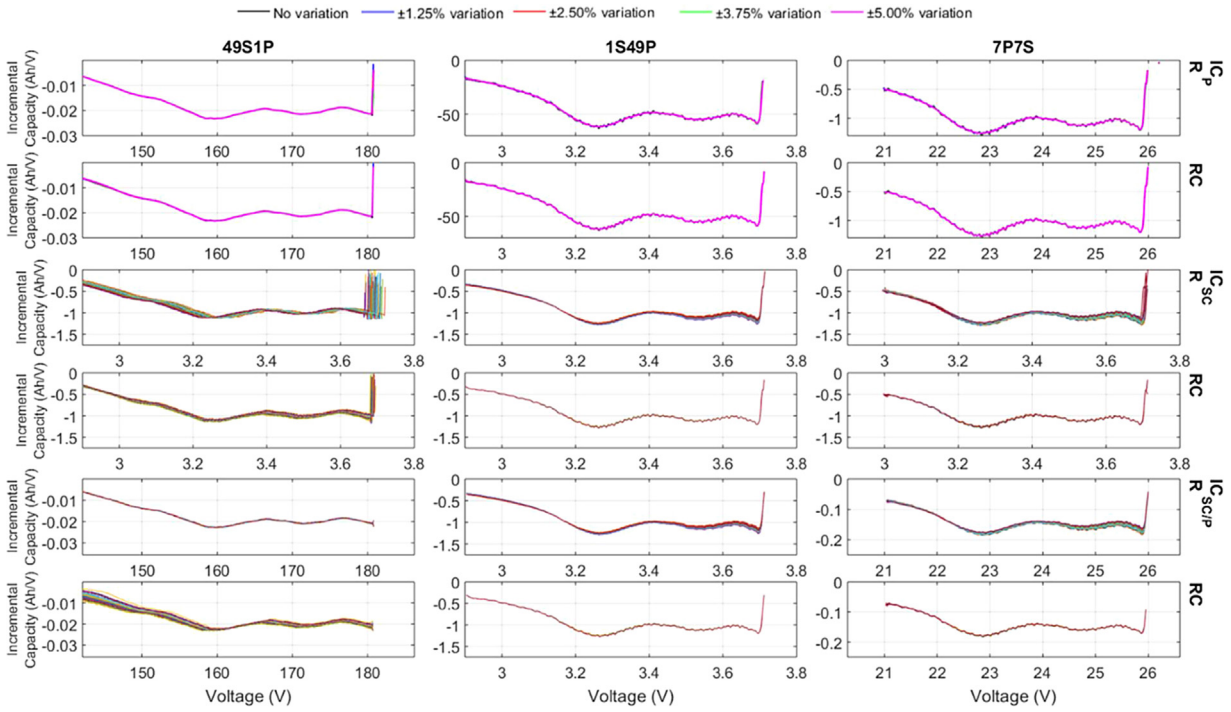

Fig. 5. NCA C/2 voltage variations induced by R and RC for the three simulated topologies. First two rows showcase the average IC signatures of the packs (10 repetitions), the third and forth rows the IC signatures of the single cells, and the fifth and sixth rows show the IC signature of the single cells on the pack voltage scale. Different colors correspond to different single cells for IC_{SC} and $IC_{SC/P}$.

and at the end of discharge. The discrepancy at the beginning of discharge was due to the different initial voltage drops within the SC; while, the discrepancy at the end of discharge was due to some SCs becoming fully discharged before the others. For RC, rate variations are overall smaller and there was more discrepancy in the middle of discharge because this is where the voltage varied the least with SOC and thus where the larger accommodations were needed to equalize all the voltages.

CtCVs were shown to have a significant impact on performance. CtCVs will differ from pack to pack and thus should be estimated in every case, if possible automatically by the BMS. Since the different CtCVs induced different voltage variations at the pack level, it might be

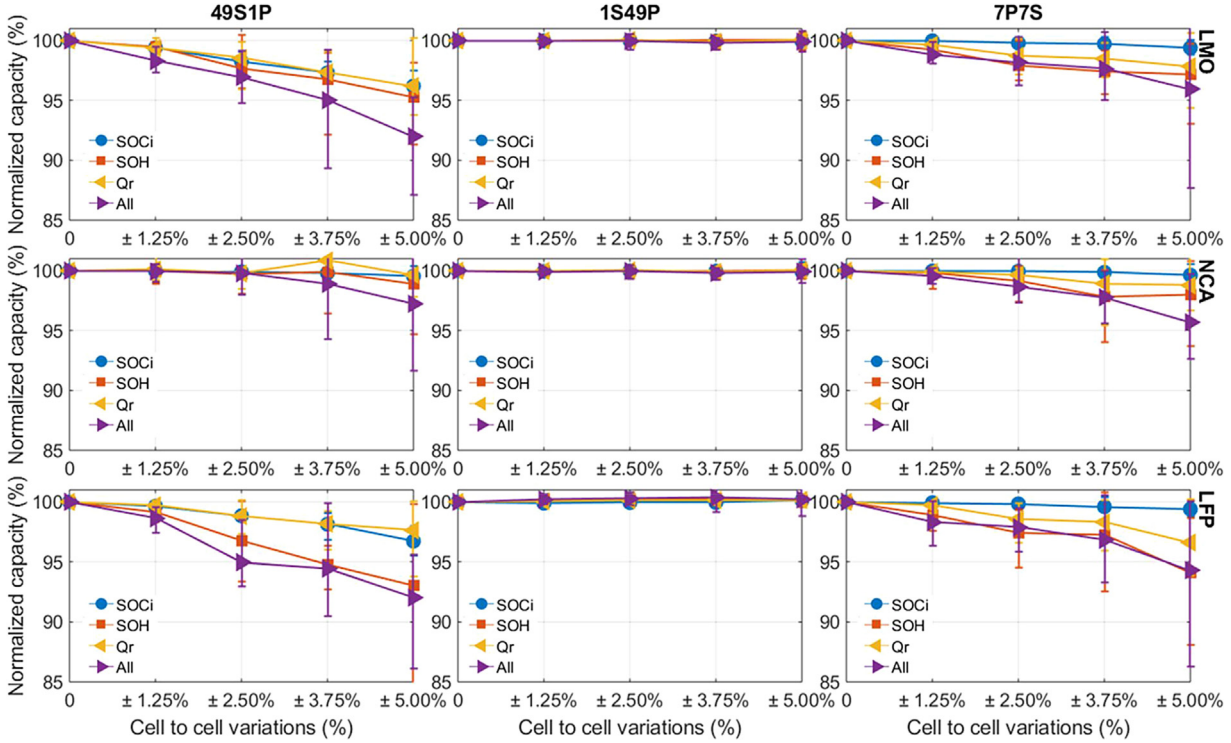

Fig. 6. Average pack C/25 capacity evolution as a function of CtCV for the four simulated topologies. Errors bars represents the deviation for the 10 repetitions for each set of conditions.

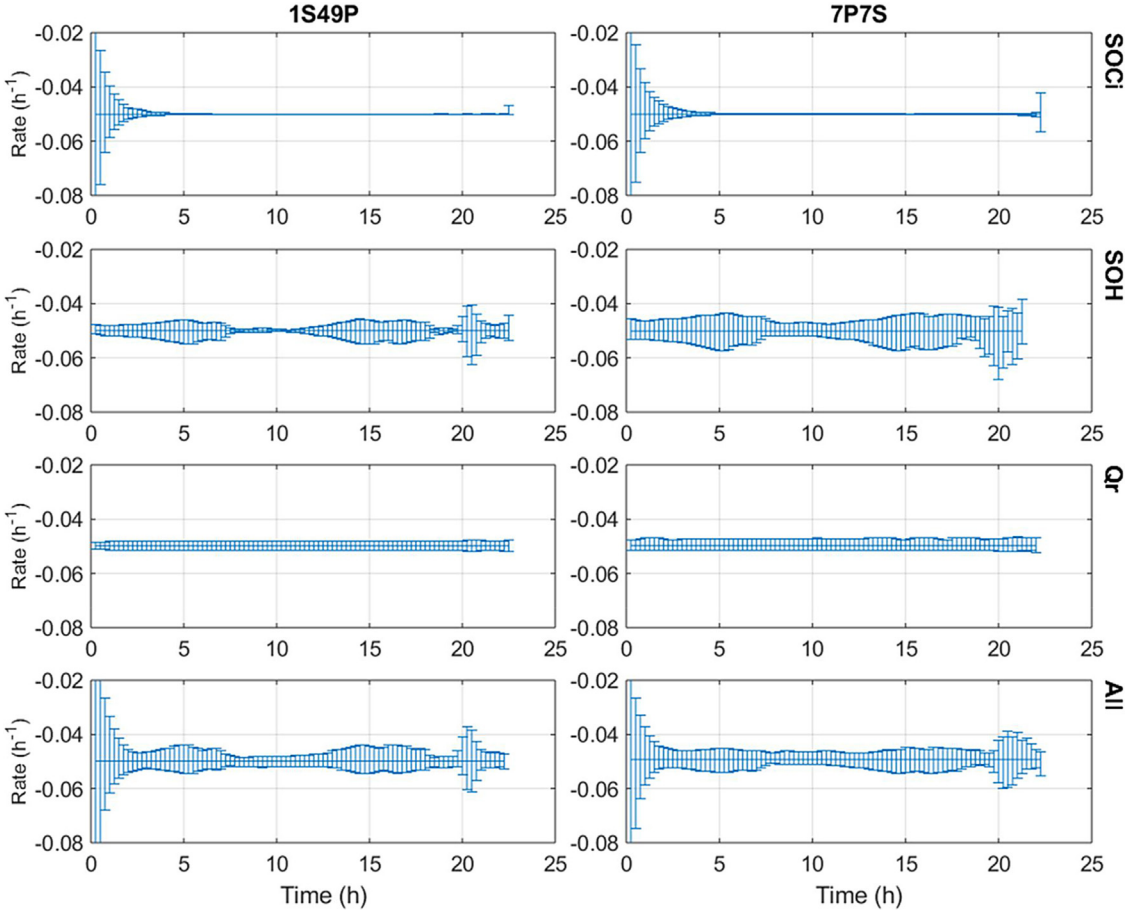

Fig. 7. LMO C/25 current variations induced by SOCi, SOH, Qr, and All CtCV for the two topologies with paralleling at the 49 single-cell level.

possible to diagnose them by analyzing the pack response. Fig. 9 plots the evolution of the FOIs as function of the degree of CtCV for SOCi, SOH, Qr, and all the variations at the same time. Variations for NCA and LFP are provided in Fig. S9. SOC variations only affected FOI2 for the 49S1P configuration. Despite showing many differences at the SC level (Fig. 3), FOI1 did not change at the pack level for 49S1P. Variations in SOH affected FOI2 for all configurations, whereas SOH variations influenced FOI3 only in 49S1P and 7P7S. Qr variations slightly affected FOI3 for all but 1S49P configuration and FOI2 for configurations with paralleling. Looking at all the variations at the same time, a full diagnosis from the voltage response at the pack level was not possible. Indeed, FOI2 and FO3 were influenced by all CtCV, but FOI1 was invariant. Moreover, the associated error bars were large and thus, the estimation was not accurate. This assessment remained true for NCA and LFP (Fig. S9).

Although the CtCV could not be quantified at the pack level, they might be at the SC level. Fig. 10 presents some automated estimations based on the All simulations, where everything was varying at the same time. Looking at SOC variations, the initial voltage was a good indicator for the 49S1P topology (Pearson's correlation coefficient $\rho = .97$ vs. $\rho < .1$ for SOH and Qr variations, respectively) but it was not for the 1S49P and 7P7S configurations ($\rho < .3$ at best) because of the initial balancing. To some degree, the SOC variations could be deciphered from the initial current for the paralleling topologies but the correlation was not as strong because it was also impacted by SOH and Qr variations ($-.97$ and $-.92$ for 1S49P and 7P7S respectively). It should be noted that the correlation decreased significantly when the rate increased to 0.66 at C/2, Fig. 11, because R and RC also affected the initial voltage and the initial current. From Fig. 3, the best option to automatically estimate the SOH was the area under the high voltage peak. Unfortunately, it was also varying with changes to Qr, with similar ρ values (in the vicinity of .9) and thus no estimation was

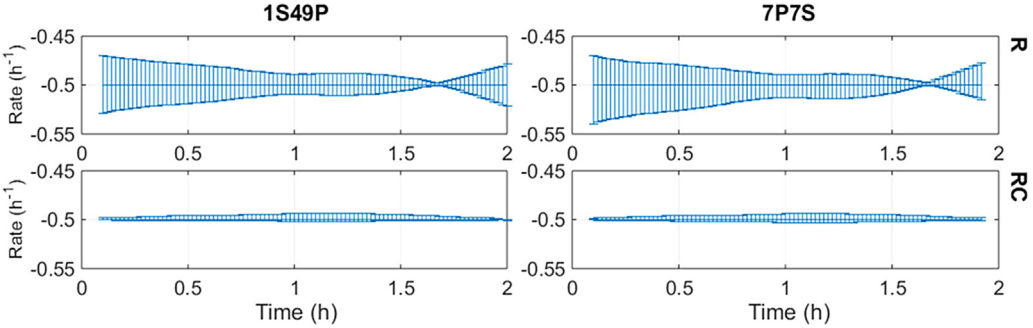

Fig. 8. NCA C/2 current variations induced by R and RC CtCV for the two topologies with paralleling at the 49 single-cell level.

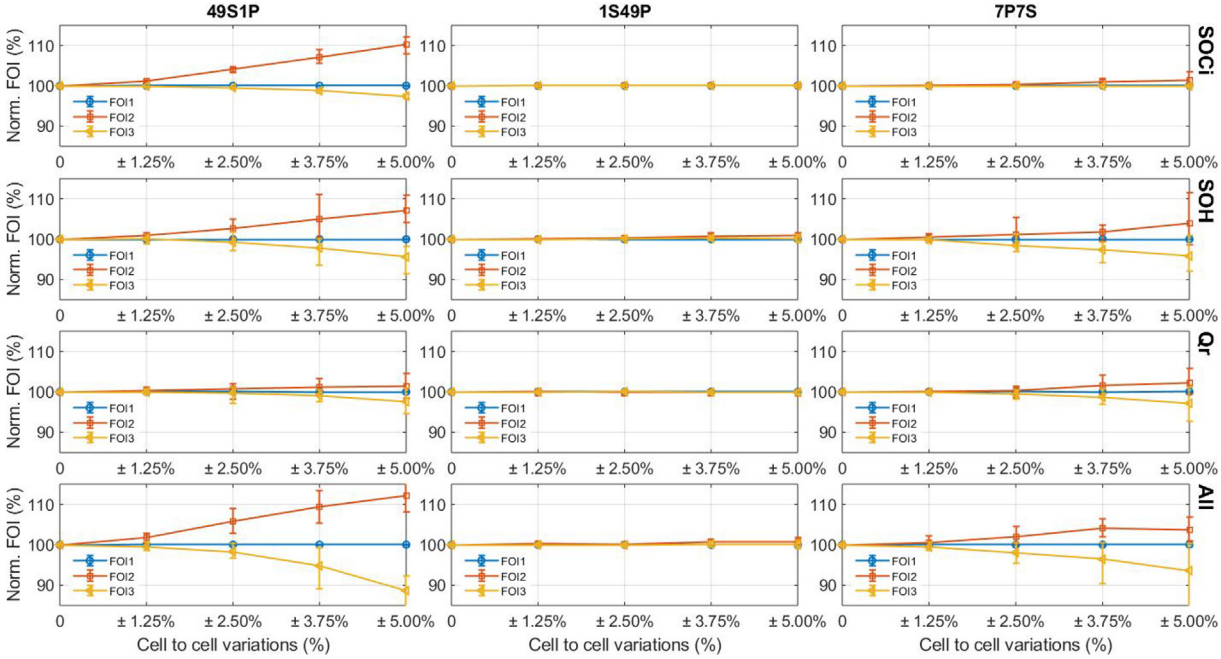

Fig. 9. LMO C/25 FOI variations as a function of the level of CtCV.

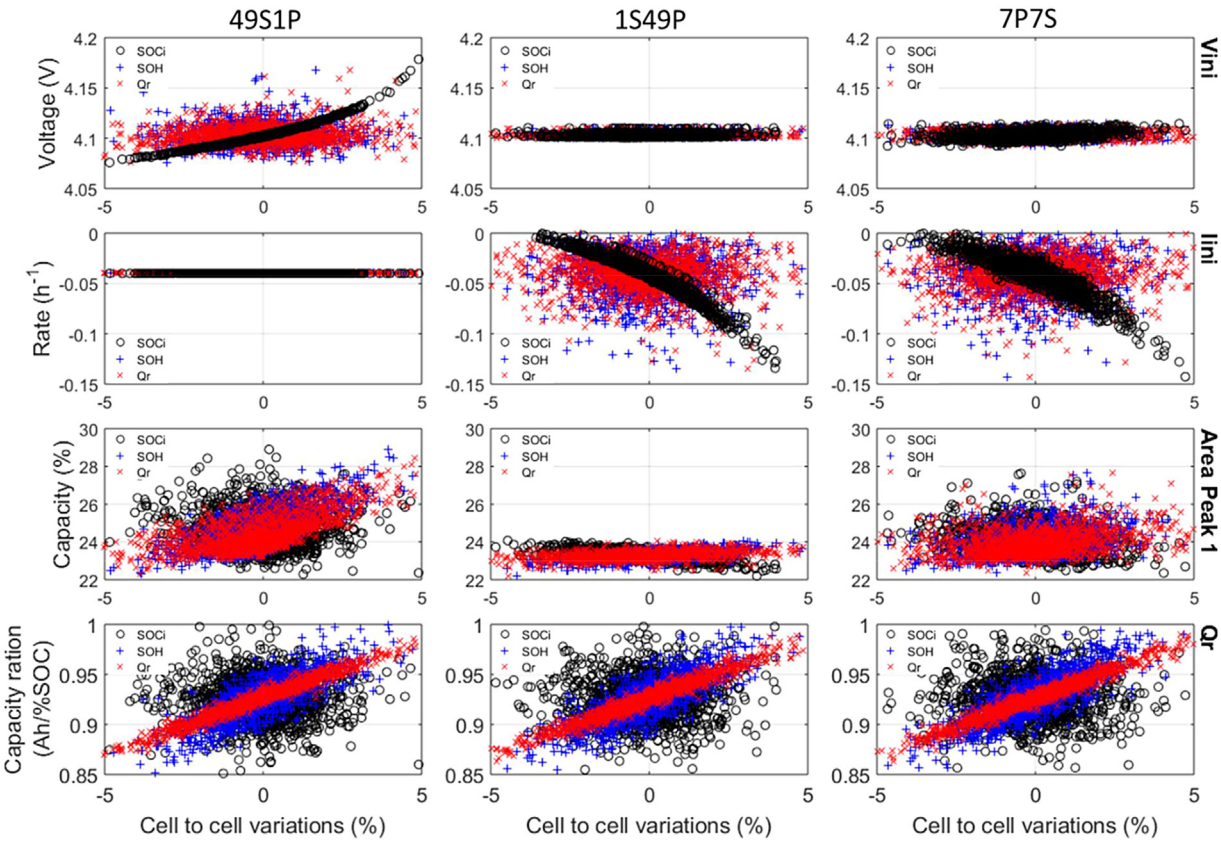

Fig. 10. Variations of the SC initial voltage (FOI1), initial current, area of the high voltage peak, and measured capacity ration as a function of the level of CtCV for LMO at C/25.

possible. Concerning the Qr, it can be estimated from the relaxation voltages before and after the discharge by calculating the associated SOC and relating them to the exchanged capacity for all topologies [3] ($\rho \sim .98$). In that case, there was also a correlation with SOH ($\rho \sim .8$) which was expected since capacity lost induce both Qr and SOH to decrease. Results were similar for NCA and LFP (Fig. S10).

5. Conclusions

This study investigated the impact of several normally distributed intrinsic CtCV, individually or as a whole, on battery pack voltage response and capacity retention. It was found that, for all chemistries, CtCV do not affect battery pack with batteries connected in parallel

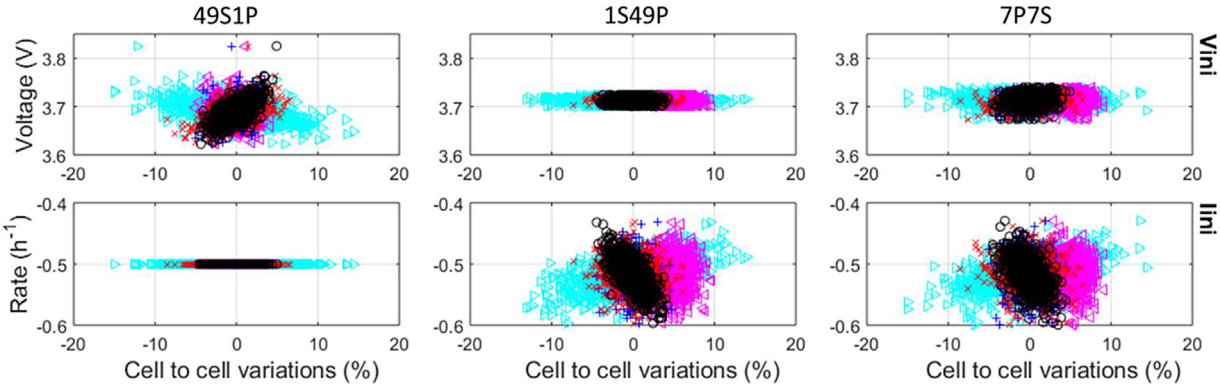

Fig. 11. Variations of the SC initial voltage (FOI1) and initial current as a function of the level of CtCV for NCA at C/2.

because of the possibility of self-balancing. When cells are connected in series, CtCV had much more of an impact on the assembly performance and that effect is chemistry dependent, NCA cells being the less affected.

The proposed methodology allowed investigating the relationship between cell quality and performance. This methodology highlights that the effect from different CtCV could be additive for packs with cells connected in series. In view of a potential BMS implementation, nothing at the pack level was deemed accurate enough for automated estimation of the CtCV from the battery pack electrochemical response. At the single-cell level, the initial SOC and Qr could be deciphered automatically at low rate but the accuracy of the estimation will drop with increasing rate because of the influences of the variations in resistance and rate capability.

Future studies could evaluate different characterization options, other types of CtCV such as different duty cycles (e.g. cell inconsistencies due to cycling) [12,14,17,27,53], operating conditions (e.g. temperature gradients), distributions (e.g. random vs. normal), and self-discharge rate. In addition, the impact of one bad cell in a batch on the performance of the entire battery pack could be investigated. Additionally, it could be interesting to change the single cell model from the alawa toolbox to a Newman type model to investigate the impact of gradients in electrode properties, such as electrode thickness, porosity, tortuosity and others on CtCVs and overall pack performance.

Author contributions

M.D. designed and implemented the model, M.D. and C.P. performed the simulations, and analyzed the data; G.B. and C.P contributed to validation and debugging. M.D. wrote the paper with inputs and proofing from G.B., C.P., T.Y., W. D.W., and J.M.

Conflicts of interest

The authors declare no conflict of interest.

Acknowledgements

This work was funded by the state of Hawaii, ONR Asia Pacific Research Initiative for Sustainable Energy Systems (APRISES) award number N00014-17-1-2206 and the Engineering and Physical Science Research Council (EPSRC – EP/I01585X/1) through the Engineering Doctoral Centre in High Value, Low Environmental Impact Manufacturing in collaboration with WMG Centre High Value Manufacturing Catapult and Jaguar Land Rover.

The authors are also grateful to the Hawaiian Electric Company for their ongoing support to the operations of the Hawai'i Sustainable Energy Research Facility (HiSERF). The authors would like to thank N. Vuillaume, C. Truchot, A. Devie, and B.Y. Liaw for their contribution in the development of the sub-models used in this work.

Appendix A. Supplementary data

Supplementary data associated with this article can be found, in the online version, at https://doi.org/10.1016/j.est.2019.02.016.

References

[1] K. Rumpf, M. Naumann, A. Jossen, Experimental investigation of parametric cell-to-cell variation and correlation based on 1100 commercial lithium-ion cells, J. Energy Storage 14 (2017) 224–243, https://doi.org/10.1016/j.est.2017.09.010.
[2] G. Lenze, H. Bockholt, C. Schilcher, L. Froböse, D. Jansen, U. Krewer, A. Kwade, Impacts of variations in manufacturing parameters on performance of lithium-ion-batteries, J. Electrochem. Soc. 165 (2) (2018) A314–A322, https://doi.org/10.1149/2.1081802jes.
[3] M. Dubarry, C. Truchot, A. Devie, B.Y. Liaw, State-of-charge determination in lithium-ion battery packs based on two-point measurements in life, J. Electrochem. Soc. 162 (6) (2015) A877–A884, https://doi.org/10.1149/2.0201506jes.
[4] F. An, L. Chen, J. Huang, J. Zhang, P. Li, Rate dependence of cell-to-cell variations of lithium-ion cells, Sci. Rep. 6 (2016) 35051, https://doi.org/10.1038/srep35051.
[5] S. Santhanagopalan, R.E. White, Quantifying cell-to-cell variations in lithium ion batteries, Int. J. Electrochem. 2012 (2012) 1–10, https://doi.org/10.1155/2012/395838.
[6] M. Dubarry, N. Vuillaume, B.Y. Liaw, Origins and accommodation of cell variations in Li-ion battery pack modeling, Int. J. Energy Res. 34 (2) (2010) 216–231, https://doi.org/10.1002/er.1668.
[7] Y. Wang, C. Zhang, Z. Chen, J. Xie, X. Zhang, A novel active equalization method for lithium-ion batteries in electric vehicles, Appl. Energy 145 (2015) 36–42, https://doi.org/10.1016/j.apenergy.2015.01.127.
[8] M. Dubarry, M. Berecibar, A. Devie, D. Anseán, N. Omar, I. Villarreal, State of health battery estimator enabling degradation diagnosis: model and algorithm description, J. Power Sources 360 (2017) 59–69, https://doi.org/10.1016/j.jpowsour.2017.05.121.
[9] L. Zhong, C. Zhang, Y. He, Z. Chen, A method for the estimation of the battery pack state of charge based on in-pack cells uniformity analysis, Appl. Energy 113 (2014) 558–564, https://doi.org/10.1016/j.apenergy.2013.08.008.
[10] Y. Wang, C. Zhang, Z. Chen, A method for joint estimation of state-of-charge and available energy of $LiFePO_4$ batteries, Appl. Energy 135 (2014) 81–87, https://doi.org/10.1016/j.apenergy.2014.08.081.
[11] D. Yang, X. Zhang, R. Pan, Y. Wang, Z. Chen, A novel Gaussian process regression model for state-of-health estimation of lithium-ion battery using charging curve, J. Power Sources 384 (2018) 387–395, https://doi.org/10.1016/j.jpowsour.2018.03.015.
[12] E. Cripps, M. Pecht, A Bayesian nonlinear random effects model for identification of defective batteries from lot samples, J. Power Sources 342 (2017) 342–350, https://doi.org/10.1016/j.jpowsour.2016.12.067.
[13] S.F. Schuster, M.J. Brand, P. Berg, M. Gleissenberger, A. Jossen, Lithium-ion cell-to-cell variation during battery electric vehicle operation, J. Power Sources 297 (2015) 242–251, https://doi.org/10.1016/j.jpowsour.2015.08.001.
[14] T. Baumhöfer, M. Brühl, S. Rothgang, D.U. Sauer, Production caused variation in capacity aging trend and correlation to initial cell performance, J. Power Sources 247 (2014) 332–338, https://doi.org/10.1016/j.jpowsour.2013.08.108.
[15] J. Kim, J. Shin, In screening process of Li-ion series battery pack for improved voltage SOC balancing, International Power Electronics Conference (2010).
[16] X. He, A facile consistency screening approach to select cells with better performance consistency for commercial 18650 lithium ion cells, Int. J. Electrochem. Sci. (2017) 10239–10258, https://doi.org/10.20964/2017.11.01.
[17] S.J. Harris, D.J. Harris, C. Li, Failure statistics for commercial lithium ion batteries: a study of 24 pouch cells, J. Power Sources 342 (2017) 589–597, https://doi.org/10.1016/j.jpowsour.2016.12.083.
[18] S. Miyatake, Y. Susuki, T. Hikihara, S. Itoh, K. Tanaka, Discharge characteristics of

multicell lithium-ion battery with nonuniform cells, J. Power Sources 241 (2013) 736–743, https://doi.org/10.1016/j.jpowsour.2013.05.179.
[19] R. Gogoana, M.B. Pinson, M.Z. Bazant, S.E. Sarma, Internal resistance matching for parallel-connected lithium-ion cells and impacts on battery pack cycle life, J. Power Sources 252 (2014) 8–13, https://doi.org/10.1016/j.jpowsour.2013.11.101.
[20] M. Dubarry, C. Truchot, M. Cugnet, B.Y. Liaw, K. Gering, S. Sazhin, D. Jamison, C. Michelbacher, Evaluation of commercial lithium-ion cells based on composite positive electrode for plug-in hybrid electric vehicle applications. Part I: Initial characterizations, J. Power Sources 196 (23) (2011) 10328–10335, https://doi.org/10.1016/j.jpowsour.2011.08.077.
[21] Y. Zheng, X. Han, L. Lu, J. Li, M. Ouyang, Lithium ion battery pack power fade fault identification based on Shannon entropy in electric vehicles, J. Power Sources 223 (2013) 136–146, https://doi.org/10.1016/j.jpowsour.2012.09.015.
[22] M. Dubarry, A. Devie, K. McKenzie, Durability and reliability of electric vehicle batteries under electric utility grid operations: bidirectional charging impact analysis, J. Power Sources 358 (2017) 39–49, https://doi.org/10.1016/j.jpowsour.2017.05.015.
[23] C. Campestrini, P. Keil, S.F. Schuster, A. Jossen, Ageing of lithium-ion battery modules with dissipative balancing compared with single-cell ageing, J. Energy Storage 6 (2016) 142–152, https://doi.org/10.1016/j.est.2016.03.004.
[24] S. Paul, C. Diegelmann, H. Kabza, W. Tillmetz, Analysis of ageing inhomogeneities in lithium-ion battery systems, J. Power Sources 239 (2013) 642–650, https://doi.org/10.1016/j.jpowsour.2013.01.068.
[25] B. Kenney, K. Darcovich, D.D. MacNeil, I.J. Davidson, Modelling the impact of variations in electrode manufacturing on lithium-ion battery modules, J. Power Sources 213 (2012) 391–401, https://doi.org/10.1016/j.jpowsour.2012.03.065.
[26] A. Devie, M. Dubarry, Durability and reliability of electric vehicle batteries under electric utility grid operations. Part 1: Cell-to-cell variations and preliminary testing, Batteries 2 (3) (2016) 28 10.3390/batteries2030028.
[27] A. Devie, G. Baure, M. Dubarry, Intrinsic variability in the degradation of a batch of commercial 18650 lithium-ion cells, Energies 11 (5) (2018), https://doi.org/10.3390/en11051031.
[28] M. Baumann, L. Wildfeuer, S. Rohr, M. Lienkamp, Parameter variations within Li-Ion battery packs – theoretical investigations and experimental quantification, J. Energy Storage 18 (2018) 295–307, https://doi.org/10.1016/j.est.2018.04.031.
[29] C. Zhang, Y. Jiang, J. Jiang, G. Cheng, W. Diao, W. Zhang, Study on battery pack consistency evolutions and equilibrium diagnosis for serial-connected lithium-ion batteries, Appl. Energy 207 (2017) 510–519, https://doi.org/10.1016/j.apenergy.2017.05.176.
[30] M. Dubarry, A. Devie, Battery durability and reliability under electric utility grid operations: representative usage aging and calendar aging, J. Energy Storage 18 (2018) 185–195, https://doi.org/10.1016/j.est.2018.04.004.
[31] C. Pastor-Fernández, T. Bruen, W.D. Widanage, M.A. Gama-Valdez, J. Marco, A study of cell-to-cell interactions and degradation in parallel strings: implications for the battery management system, J. Power Sources 329 (2016) 574–585, https://doi.org/10.1016/j.jpowsour.2016.07.121.
[32] Y. Zhao, W. Zhang, J. Jiang, T. Zhao, F. Wen, Analysis on inconsistency of electric bicycle battery pack, 2014 IEEE Conference and Expo Transportation Electrification Asia-Pacific (ITEC Asia-Pacific), Beijing, China, IEEE, Beijing, China, 2014, pp. 1–5, , https://doi.org/10.1109/ITEC-AP.2014.6941063.
[33] Y. Jiang, J. Jiang, C. Zhang, W. Zhang, Y. Gao, Q. Guo, Recognition of battery aging variations for $LiFePO_4$ batteries in 2nd use applications combining incremental capacity analysis and statistical approaches, J. Power Sources 360 (2017) 180–188, https://doi.org/10.1016/j.jpowsour.2017.06.007.
[34] T. Bruen, J. Marco, Modelling and experimental evaluation of parallel connected lithium ion cells for an electric vehicle battery system, J. Power Sources 310 (2016) 91–101, https://doi.org/10.1016/j.jpowsour.2016.01.001.
[35] C.-Y. Chang, P. Tulpule, G. Rizzoni, W. Zhang, X. Du, A probabilistic approach for prognosis of battery pack aging, J. Power Sources 347 (2017) 57–68, https://doi.org/10.1016/j.jpowsour.2017.01.130.
[36] J. Lee, J.-H. Ahn, B.K. Lee, A novel Li-ion battery pack modeling considering single cell information and capacity variation, 2017 IEEE Energy Conversion Congress and Exposition (ECCE), Cincinnati, OH, USA, IEEE, Cincinnati, OH, USA, 2017, pp. 5242–5247, , https://doi.org/10.1109/ECCE.2017.8096880.
[37] K. Rumpf, A. Rheinfeld, M. Schindler, J. Keil, T. Schua, A. Jossen, Influence of cell-to-cell variations on the inhomogeneity of lithium-ion battery modules, J. Electrochem. Soc. 165 (11) (2018) A2587–A2607, https://doi.org/10.1149/2.0111811jes.
[38] M. Dubarry, N. Vuillaume, B.Y. Liaw, From Li-ion single cell model to battery pack simulation, 17th IEEE International Conference on Control Applications, San Antonio, TX, 2008, pp. 708–713.
[39] M. Dubarry, A. Devie, B.Y. Liaw, Cell-balancing currents in parallel strings of a battery system, J. Power Sources 321 (2016) 36–46, https://doi.org/10.1016/j.jpowsour.2016.04.125.
[40] L. Zhou, Y. Zheng, M. Ouyang, L. Lu, A study on parameter variation effects on battery packs for electric vehicles, J. Power Sources 364 (2017) 242–252, https://doi.org/10.1016/j.jpowsour.2017.08.033.
[41] L. Zhou, Y. Zheng, M. Ouyang, L. Lu, A simulation study on parameter variation effects in battery packs for electric vehicles, Energy Procedia 105 (2017) 4470–4475, https://doi.org/10.1016/j.egypro.2017.03.949.
[42] M. Dubarry, G. Baure, C.P. Fernández, T.F. Yu, D. Widanage, J. Marco, Battery energy storage system modeling: a combined comprehensive approach, J. Energy Storage 21 (2019) 172–185, https://doi.org/10.1016/j.est.2018.11.012.
[43] M. Dubarry, V. Svoboda, R. Hwu, B.Y. Liaw, Incremental capacity analysis and close-to-equilibrium OCV measurements to quantify capacity fade in commercial rechargeable lithium batteries, Electrochem. Solid-State Lett. 9 (10) (2006) A454–A457, https://doi.org/10.1149/1.2221767.
[44] M. Dubarry, C. Truchot, B.Y. Liaw, Synthesize battery degradation modes via a diagnostic and prognostic model, J. Power Sources 219 (2012) 204–216, https://doi.org/10.1016/j.jpowsour.2012.07.016.
[45] HNEI Alawa Central. https://www.soest.hawaii.edu/HNEI/alawa/ (March).
[46] M. Dubarry, N. Vuillaume, B.Y. Liaw, From single cell model to battery pack simulation for Li-ion batteries, J. Power Sources 186 (2) (2009) 500–507, https://doi.org/10.1016/j.jpowsour.2008.10.051.
[47] M. Dubarry, G. Baure, A. Devie, Durability and reliability of EV batteries under electric utility grid operations: path dependence of battery degradation, J. Electrochem. Soc. 165 (5) (2018) A773–A783, https://doi.org/10.1149/2.0421805jes.
[48] D. Anseán, M. Dubarry, A. Devie, B.Y. Liaw, V.M. García, J.C. Viera, M. González, Operando lithium plating quantification and early detection of a commercial $LiFePO_4$ cell cycled under dynamic driving schedule, J. Power Sources 356 (2017) 36–46, https://doi.org/10.1016/j.jpowsour.2017.04.072.
[49] D. Anseán, M. Dubarry, A. Devie, B.Y. Liaw, V.M. García, J.C. Viera, M. González, Fast charging technique for high power $LiFePO_4$ batteries: a mechanistic analysis of aging, J. Power Sources 321 (2016) 201–209, https://doi.org/10.1016/j.jpowsour.2016.04.140.
[50] ElectroPapa Li-Ion-battery – 6600mAh (2.5V) black – for laptop 73notebook replaces BAT-1S3P. https://electropapa.com/en/li-ion-battery-6600mah-2-5v-black-for-laptop-n.utm (8/9/2018).
[51] Dell Specications Dell Latitude E6220. https://data.technimax.cz/attach/artilky/Dell-Latitude-E6220-parametry.pdf (8/9/2018).
[52] EObsession, Tesla Roadster specifications, https://evobsession.com/tesla-roadster-specs-history-prices/(8/9/2018).
[53] S. Rohr, S. Müller, M. Baumann, M. Kerler, F. Ebert, D. Kaden, M. Lienkamp, Quantifying uncertainties in reusing lithium-ion batteries from electric vehicles, Procedia Manuf. 8 (2017) 603–610, https://doi.org/10.1016/j.promfg.2017.02.077.